CCFE
CULHAM CENTRE FOR FUSION ENERGY

UK Atomic Energy Authority

UKAEA-CCFE-CP(22)09

A. Shepherd, B. Pouradier Duteil, T. Patton, A. Rigoni, G. Serianni, E. Sartori. A. Pimazzoni

Initial results from the SPIDER beamlet current diagnostic

Initial results from the SPIDER beamlet current diagnostic

A. Shepherd, B. Pouradier Duteil, T. Patton, A. Rigoni, G. Serianni,
E. Sartori. A. Pimazzoni

This paper has been submitted to
2021 IEEE Pulsed Power Conference & Symposium on Fusion Engineering (PPC/SOFE) NPSS, Denver, Colarado, USA, 12-16 December 2021

Initial Results from the SPIDER Beamlet Current Diagnostic

A. Shepherd, B. Pouradier Duteil, T. Patton, A. Rigoni, G. Serianni, E. Sartori, A. Pimazzoni

***Abstract*—SPIDER (Source for the Production of Ions of Deuterium Extracted from a Radio frequency plasma) is the full-scale prototype for the ITER Heating Neutral Beam (HNB) source. Driven by four driver coil pairs powered by oscillators the SPIDER source plasma exhibits fluctuations in the range of kHz to MHz, as observed by Langmuir probes and Source Emission Spectroscopy. These fluctuations are believed to influence the extracted beam current, meniscus shape and beam features. Beam operation in SPIDER, with the eventual aim of achieving 100 keV, 46 A hydrogen negative ion beam for one hour, has mainly been performed in volume operation without cesium. Recently, with the introduction of cesium, SPIDER has moved to the surface operational regime, with a noted increase in beam current. Electrical and calorimetric measurements of the beam current have previously shown discrepancies between the two, possibly due to background gas interactions in the accelerator and upstream of the STRIKE calorimeter. Taking advantage of the reduced number of beamlets due to the Plasma Grid mask a series of Hall Effect current transducers and AC current transformers have been installed in SPIDER. These Beamlet Current Monitors (BCMs), positioned downstream of the Grounded Grid around individual grid apertures, provide a direct measurement of the current of up to five individual beamlets, from DC up to 5MHz frequencies. This contribution describes the initial results from the BCM with and without cesium, focusing on the characterization of the beamlet direct current component.**

***Index Terms*—SPIDER, beam current, inhomogeneity**

I. INTRODUCTION

SPIDER [1] (Source for the Production of Ions of Deuterium Extracted from a Radio frequency plasma) is the full-scale prototype for the ITER Heating Neutral Beam (HNB) source. Operating at the Neutral Beam Test Facility (NBTF) in Padova, Italy, its main purpose is to optimize the ITER HNB Ion Source, which has a requirement of 355 A/m^2 in hydrogen and 290 A/m^2 in deuterium with a uniformity of ±10 %.

The plasma inside the SPIDER Ion Source is created by eight driver coils in a 4x2 array, paired horizontally and powered by four 200 kW oscillators. The SPIDER RF generators oscillate around 1 MHz ±0.1 MHz, with a variable capacitance C_v adjusted to match the load impedance. Due to variations in the driver plasma load, and restrictions in the available frequency range due to frequency flips [2], the self-oscillation frequency between generators can vary on the range of kHz.

Plasma generated within the eight drivers expands into the expansion chamber, enclosed by the Plasma Grid (PG). Negative ions are generated within the source either through volume production mechanisms or with the addition of evaporated cesium, surface mechanisms [3]. To reduce the electron temperature near the PG and minimise H- dissociation a vertical current I_{PG} is passed through the PG to produce a transverse filter field (FF) within the expansion chamber.

Negative ions are extracted and accelerated through a stack of three copper electrostatic grids: consisting of the PG, Extraction Grid (EG) and Grounded Grid (GG). The PG is kept at source potential $U_{source} = -U_{ext}-U_{acc}$ and the EG at $U_{EG} = -U_{acc}$. The extraction and acceleration voltages U_{ext} and U_{acc} are the potential differences between the grids, with limits of 12 kV and 96 kV respectively.

Electrons are also extracted from the ion source, which are deflected onto the EG by permanent magnets embedded in the EG and the downstream field generated by I_{PG}. An electron-to-ion ratio $e/H^- < 1$ is required to protect the EG from excessive heat loads. To further reduce the electron density near the PG independent positive bias voltages are applied to the PG (BI) and to a dedicated bias plate (BP).

The SPIDER accelerator is composed of 1280 individual beamlets, grouped into four vertical segments. Each segment consists of four horizontal groups of 80 beamlets with 15 rows and 5 columns. Gas is fed into the SPIDER source through the eight drivers, where the neutral background gas expands through the grid stack into the vacuum vessel. At ITER relevant source pressures the SPIDER vacuum system has been unable to keep the vessel pressure low enough to prevent breakdowns at the back of the source [4]. To reduce the gas conductance through the accelerator a mask has been installed upstream of the PG that reduces the number of open apertures [5]. Three

This work has been carried out within the framework of the EUROfusion Consortium and has received funding from the Euratom research and training programme 2014-2018 and 2019-2020 under grant agreement No 633053. The views and opinions expressed herein do not necessarily reflect those of the European Commission. This work has been carried out within the framework of the ITER-RFX Neutral Beam Testing Facility (NBTF) Agreement and has received funding from the ITER Organization. The views and opinions expressed herein do not necessarily reflect those of the ITER Organization.

Corresponding author: A. Shepherd

A. Shepherd is with Culham Centre for Fusion Energy (CCFE), Culham Science Centre, Abingdon, Oxfordshire, OX14 3DB, UK, seconded to Consorzio RFX, Corso Stati Uniti 4, 35127, Padova, Italy (email: alastair.shepherd@igi.cnr.it).

B. Pouradier Duteil is with Ecole Polytechnique Fédérale de Lausanne (EPFL), Swiss Plasma Center (SPC), 1015 Lausanne, Switzerland, seconded to Consorzio RFX, Corso Stati Uniti 4, 35127, Padova, Italy (email: basile.duteil@igi.cnr.it).

T. Patton, A. Rigoni, G. Serianni, E. Sartori and A. Pimazzoni are with Consorzio RFX, Corso Stati Uniti 4, 35127, Padova, Italy (email: tommaso.patton@igi.cnr.it; andrea.rigoni@igi.cnr.it; gianluigi.serianni@igi.cnr.it; emanuele.sartori@igi.cnr.it; antonio.pimazzoni@igi.cnr.it.).

E. Sartori is also with Università degli Studi di Padova, Padova, Italy.

masks have been used up to now, the first two reducing the number of open apertures to 80 and the current mask to 28 apertures.

Until the recent cesium campaign the negative ions have been generated inside the source via volume production mechanisms, with an H^- current density $J_{H^-} = 30$ A/m^2. The beam current measured using STRIKE electrical and calorimetric measurements, and the current drained by the acceleration grid power supply (AGPS), have given different results [6], and so a measurement of the direct beam current is desirable.

The frequency differences between the four oscillators can drive instabilities in the plasma at the 'beat' frequencies of the oscillators, the frequency difference between a pair of oscillators. Additional fluctuations have been observed by source diagnostics at the oscillator harmonic frequencies (MHz range). These fluctuations can affect the plasma near the PG including the meniscus, with a subsequent impact on the beam current and divergence.

Taking advantage of the individual beamlets due to the SPIDER PG mask a diagnostic has been developed, the Beamlet Current Monitor (BCM) [7], that can measure the beamlet current up to 30 mA with a 1 mA resolution and DC to 5 MHz range. Using the BCM the trends of the beamlet DC current with the SPIDER source parameters have been assessed in both volume and surface H^- production regimes.

II. Experimental Setup

The BCM diagnostic consists of five sensor modules (Fig. 1a). Closest to the Grounded Grid (GG) is a DC sensor, followed by a current transformer to provide AC measurements up to 5 MHz. Finally, a positively biased repeller disk prevents backstreaming positive ions from entering the sensor.

The DC sensor consists of a LEM CTSR 0.3p closed loop fluxgate [8] (Fig. 1b), with a 4 V/A gain and a DC to 10 kHz bandwidth (-3 dB). As the sensor has a large non-zero offset, a conditioning circuit consisting of a INA 114 amplifier has been added to reduce the offset and increase the sensor gain to 245-267 V/A (depending on the individual sensor).

The five BCM modules are installed downstream GG, attached to the pusher structure that holds the PG mask in place (Fig. 2). The mask reduces the number of available beamlets from 1280 to 28 to reduce conductance through the grid stack and lower the vessel pressure. The sensors are positioned such that there is a measurement in each segment row, with examples of beamlets at the edge and core of a segment.

III. DC Signal Analysis

A Red Pitaya digital oscilloscope acquires the voltage measured by the individual DC sensors, with the processed signal stored in the SPIDER MDSPlus pulse file. The voltage (black points in Fig. 3a) has a noise of ±1.5 V and is filtered (red line in Fig. 3a) for the analysis. Being a magnetic fluxgate, the sensor voltage is sensitive to stray magnetic fields and the source plasma as well as the H^- beam. The sensor voltage in Fig. 3a changes with the RF power (highlighted green in Fig. 3a and d), the current flowing through the plasma grid I_{PG} (highlighted blue in Fig. 3a and d), U_{ext} and U_{acc} (highlighted red in in Fig. 3a and d).

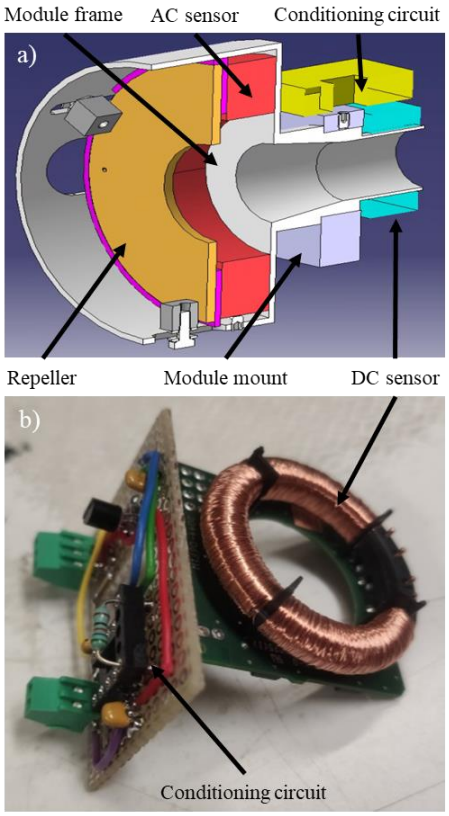

Fig. 1. a) BCM module, in order from nearest to the GG; DC sensor, AC sensor and repeller disk. b) DC sensor consisting of LEM CTSR 0.3p and conditioning circuit.

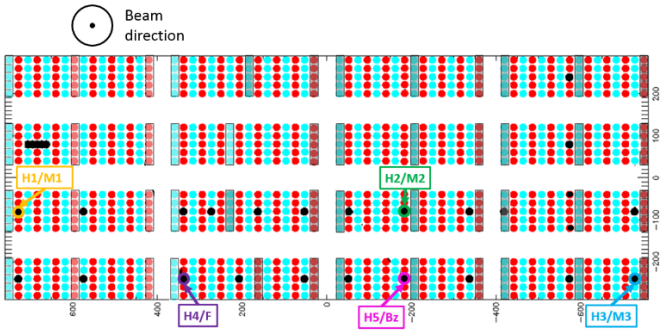

Fig. 2. Position of the five BCM modules downstream of the SPIDER GG (grid turned horizontal). Black points indicate the 28 unmasked beamlets.

A steady baseline with constant source parameters (black in Fig. 3b) is therefore required to calculate the beamlet current from the voltage increase due to the beam (red in Fig. 3b). The beamlet current $I_{beamlet}$ (blue in Fig. 3c) is given by equation (1).

$$I_{beamlet} = {(V_{beamlet} - V_{baseline})}/{G_s} \qquad (1)$$

G_s is the voltage/current gain of each individual sensor. The current is averaged at each Time of Interest (TOI) for the analysis (red points in Fig. 3c). It should be noted that the BCM measures the accelerated current that exits the GG and not the extracted current for each beamlet, which due to beam transmission will be larger.

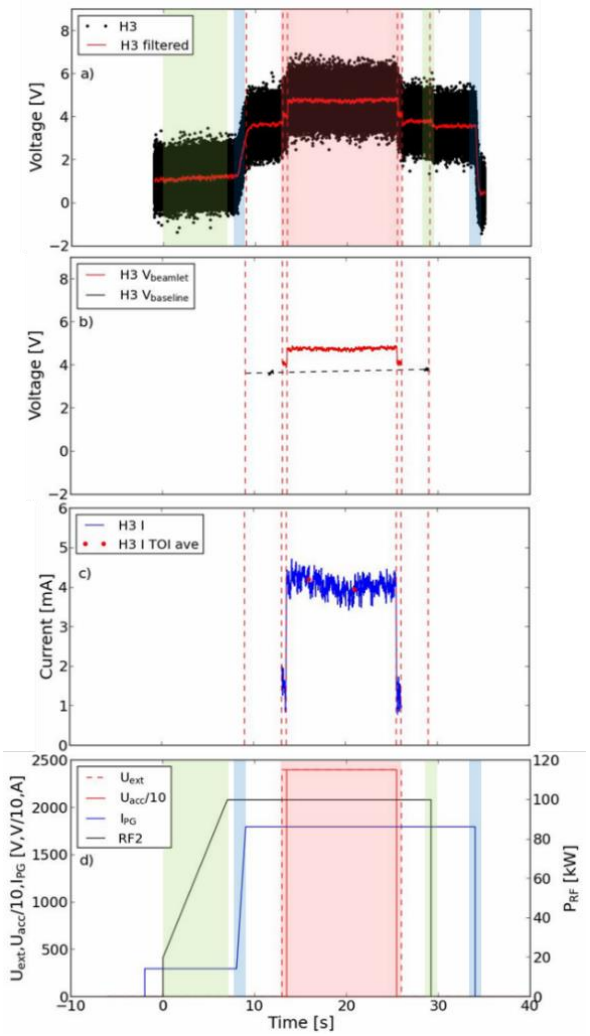

Fig. 3. Sensor H3 DC signal analysis for pulse 8776. a) Raw and filtered voltage signal, b) voltage baseline and voltage due to beam, c) calculated beamlet current with the average at the TOIs marked in red, d) SPIDER source reference parameters.

IV. BEAM CHARACTERIZATION DURING VOLUME OPERATION

SPIDER operation before May 2021 has been dedicated to characterization of the SPIDER beam in hydrogen with the source in volume operation, i.e. without cesium. The filter field has been operated in two configurations, standard with I_{PG} directed downwards through the PG, and reversed with I_{PG} upwards.

A. Extraction Voltage Trends

The averaged BCM currents, taken at the last TOI of each beam on phase, are shown for a scan in extraction voltage U_{ext}, in the standard and reversed filter field configurations (Fig. 4). As expected the beamlet current densities increase with U_{ext}, following the Child-Langmuir law. In the standard configuration the beamlet at the bottom of the GG, H3, has the lowest current, and indeed reaches saturation at 1.7 kV. This top-bottom inhomogeneity, due to diamagnetic and ExB drift caused by the magnetic filter field in the source expansion

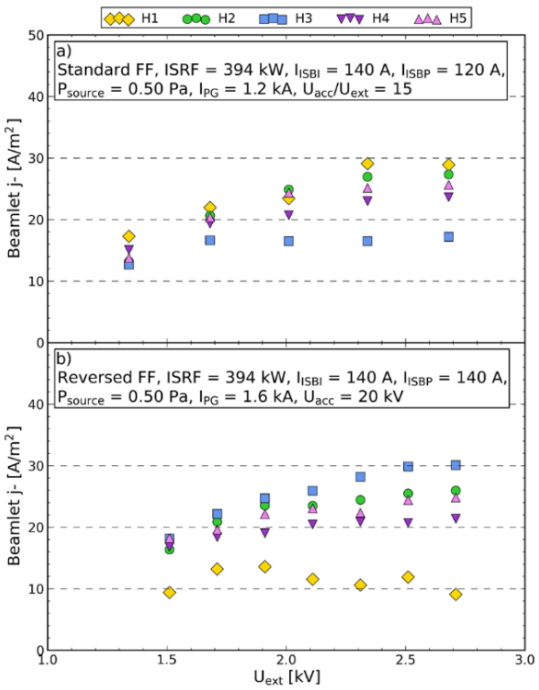

Fig. 4. Extraction voltage scans for a) standard and b) reversed FF configurations in volume operation.

region is to be expected and has been observed by visible cameras [9] and STRIKE [10].

Reversing the filter field switches vertical asymmetry such that the top beamlet (H1) becomes the lowest. This confirms that the asymmetry is due to the influence of the filter field. The behavior is not perfectly symmetrical between the two configurations, with H1 noticeably lower than the other beamlets in the reversed configuration at all U_{ext}, and decreasing above 2 kV.

The standard configuration scan was carried out at a fixed U_{acc}/U_{ext} while the reversed configuration scan at a fixed U_{acc}. This could result in increased beamlet scraping on the GG for beamlet H1 as the beamlet optics deteriorates at low U_{acc}/U_{ext}, explaining the decreasing current.

B. Filter Field Trends

I_{PG} is also different in the two extraction scans, and the strength of the filter field has a strong effect on the beamlet currents (Fig. 5). In both configurations, the peak beamlet current is around 1.1-1.3 kA, with the current decreasing at higher filter field. However in the standard configuration the lowest beamlet H3 is closer to the other beamlets beyond 1.1 kA, compared to the highest beamlet H1 in the reversed configuration. The standard configuration therefor appears to be the preferred filter field orientation for producing a more vertically homogeneous beam.

Measurements of the beamlet vertical profile using STRIKE [10] have shown that there is a ‘bell shape’ non-uniformity within beamlet groups, which increases with the filter field. The measurements with the BCM, while not able to give a complete vertical profile of the beam due to the limited number of sensors, confirms this general trend. Normalizing each beamlet group current (Fig. 6), the beamlets at the edge of their

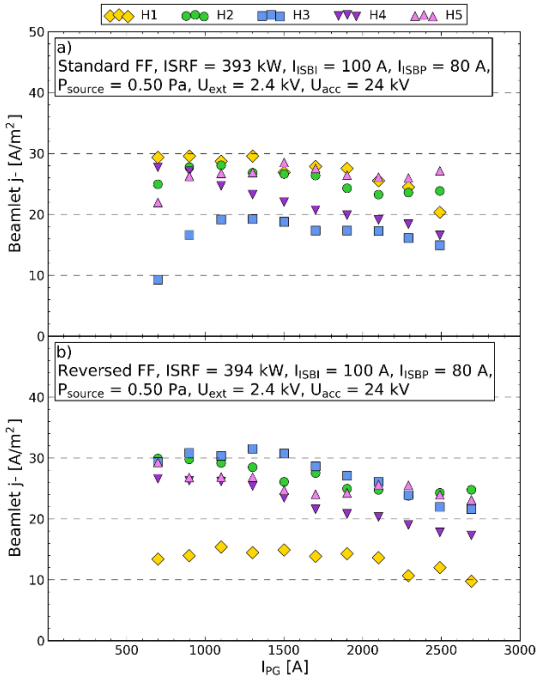

Fig. 5. FF current scans for a) standard and b) reversed FF configurations in volume operation.

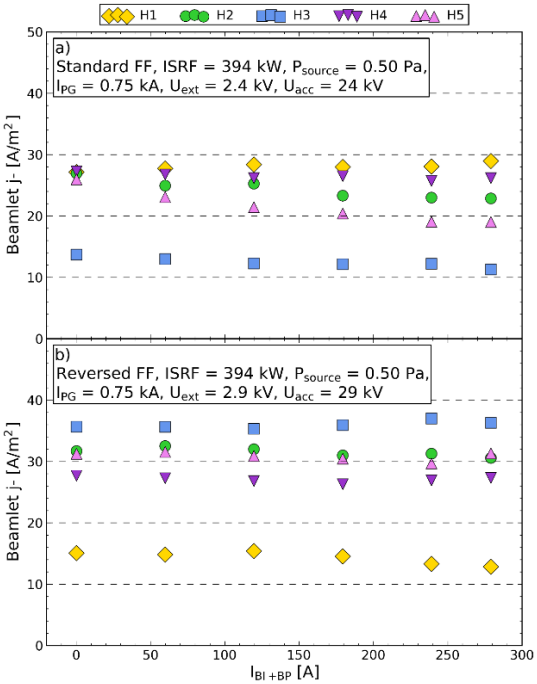

Fig. 7. Bias current scans for: a) standard and b) FF configurations at I_{PG} = 0.75 kA in volume operation.

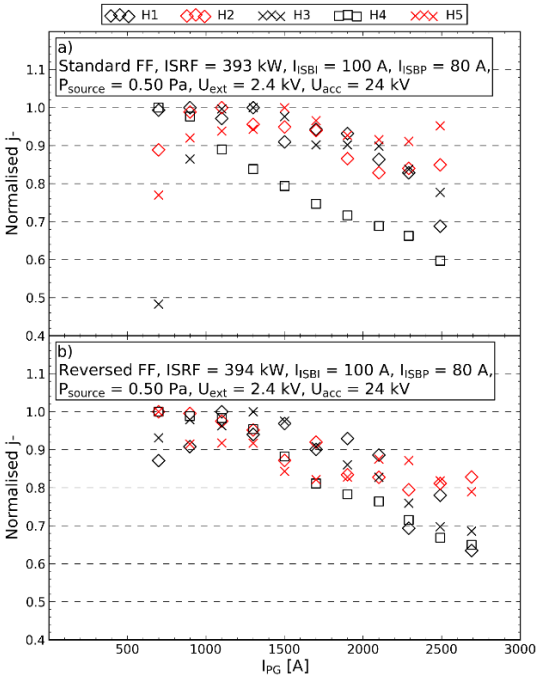

Fig. 6. Normalized filter field current scans for: a) standard filter field and b) reversed FF configurations in volume operation.

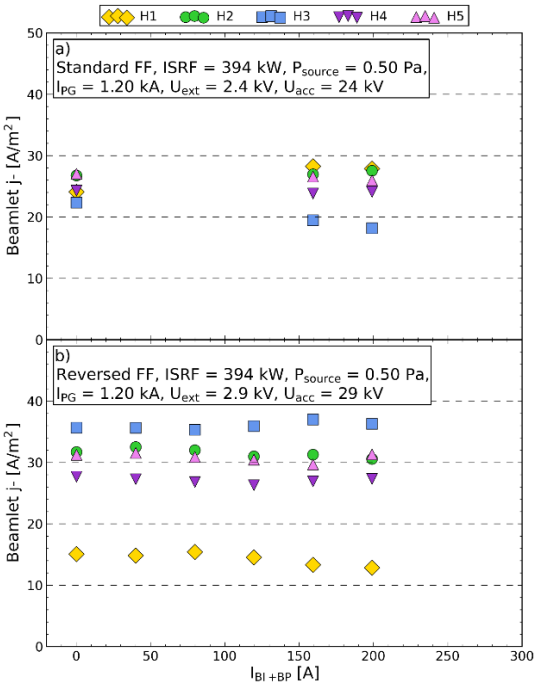

Fig. 8. Bias current scans for: a) standard and b) reversed FF configurations at IPG = 1.20 kA in volume operation.

respective beamlet groups (H1, H3 and H4 in black) are more strongly influenced by the filter field than the ones in the beamlet group cores (H2 and H5 in red).

C. Bias Trends

On SPIDER, the PG (BI) and bias plate (BP) are biased independently, controlled by either voltage or current. Increasing the total bias current I_{BI+BP} shows a mild increase in the vertical asymmetry in both filter field configurations (Fig. 7 and Fig. 8). The spreading in beamlet currents appears stronger in the standard FF direction and at lower PG currents.

V. MONITORING THE CESIUM EFFECT DURING SURFACE OPERATION

As mentioned previously the beamlet current follows the Child-Langmuir law, where the extracted current density due to

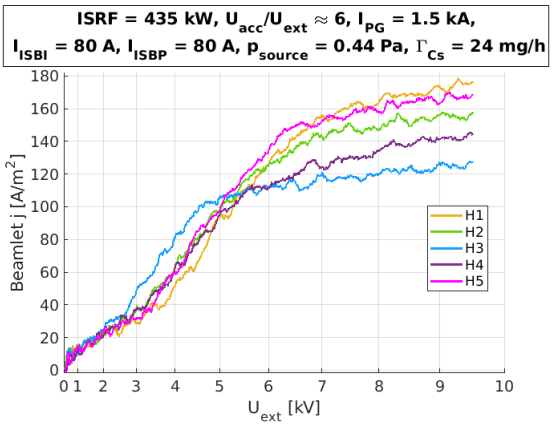

Fig. 9. Current density measurements of the five BCM beamlets during an extraction voltage scan in surface operation. The x-axis has been modified to show U_{ext} instead of $U_{ext}^{3/2}$.

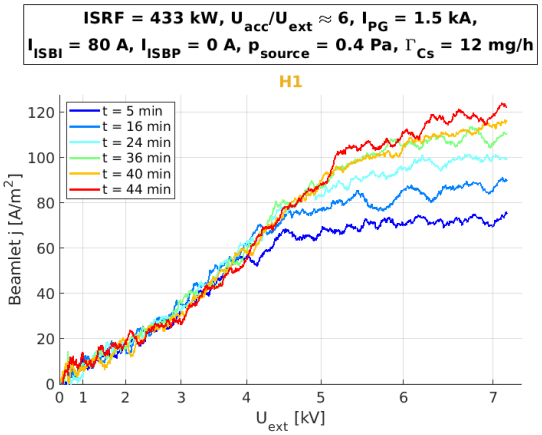

Fig. 10. Extraction voltage scans of a single beamlet for the first six identical pulses of an experimental day. The steady-state appears to be reached at t ≈ 40 min.

voltage U_{ext} is limited by the beam space-charge, assuming an unlimited ion source. In the case of a parallel plane diode, the maximum extracted current density is given by equation (2).

$$J_i^{CL} = \frac{4\epsilon_0}{9d^2}\sqrt{\frac{2q}{m_i}}\,U_{ext}^{3/2} \qquad (2)$$

Where d is the distance between anode and cathode, q the ion's electrical charge and m_i the ion's mass. The beamlet current measured by the BCM follows a linear dependence on $U_{ext}^{3/2}$ (Fig. 9) while there are available negative ions for extraction, as stated by (2). The slope differs from one beamlet to another, due to its dependency on the local extraction gap geometry and the plasma meniscus. At higher U_{ext} the current saturates due to a limit in the available negative ion density. The different saturation currents for different beamlets indicate a non-uniformity in the availability of negative ions, either due to non-uniformity in the plasma or cesiation state.

With monitoring of the beamlet currents at the beginning of the experimental day, an indication of the cesium status can be acquired (Fig. 10). During U_{ext} scans within repeated plasma pulses the beamlet current rises due to an increase in the available negative ion density as the cesium condition improves. After several plasma pulses the current starvation reaches a steady state, implying the ceasiation has also reached steady state. In conjunction with the Ion Source Extraction Grid (ISEG) current, as an indication of the saturation of the co-extracted electron current, the diagnostic is used to determine when the cesium condition is stable enough to carry out experimentation of the beam and source parameters.

VI. BEAM CHARACTERIZATION DURING SURFACE OPERATION

The introduction of cesium to the SPIDER source switches the primary H- production method from volume to surface processes. The resulting increase in average H- current is 25 A/m2 to 140 A/m2 when the total RF power into the source is 400 kW (Fig. 10).

In surface operation, the observed trends with the filter field in the standard configuration are similar to volume operation (Fig. 12). The vertical non-uniformity in the beamlet current matches the volume operation case (Fig. 4a), with the beamlet at the bottom of segment 4, H3, lower than the others. Increasing U_{ext} increases the non-uniformity due to the lower H^- availability for extraction at the bottom of the source. However, at 4 kV the vertical non-uniformity appears to be reversed with H3 highest. The cause of this switch is due to the poorer beam transmission for the beamlets with larger saturation currents (all but H3) at low U_{ext}, which causes scraping on the EG.

The effect of the filter field appears more pronounced in surface operation, with all of the beamlet currents except H3 decrease considerably, including the core beamlets (H2 and H5), albeit over a limited I_{PG} range. Increasing the bias increases the top- bottom asymmetry due to the plasma drift, as seen in volume operation.

VII. CONCLUSIONS

Since its installation in early 2021 the Beamlet Current Monitor has provided a direct, non-invasive measurement of the SPIDER beamlet current. In volume operation currents of over 30 A/m^2 have been observed, with a clear inhomogeneity in the vertical current profile. This inhomogeneity is dependent on the filter field direction, confirmed by other SPIDER beam diagnostics. The trends in beam current with SPIDER source parameters are clear and consistent with measurements made with STRIKE [10], Beam Emission Spectroscopy and visible cameras [9].

During the first SPIDER experimental campaign with cesium the BCM has been an important diagnostic for monitoring the cesium condition through the beamlet current. By assessing the Child-Langmuir curve for the measured beamlets, not only can the status of the cesiation process be judged in near real time, but also the required extraction voltage to reach current saturation can be obtained. This allows U_{ext} to be fixed before performing scans of other source parameters.

The measured beamlet current during surface operation has risen to over 150 A/m2 for some beamlets. The trends with SPIDER source parameters follow those observed in volume operation for similar RF power. From the scans analyzed the beam uniformity is optimal around U_{ext} = 5 kV, while the beamlets are still mostly space-charge limited. At higher

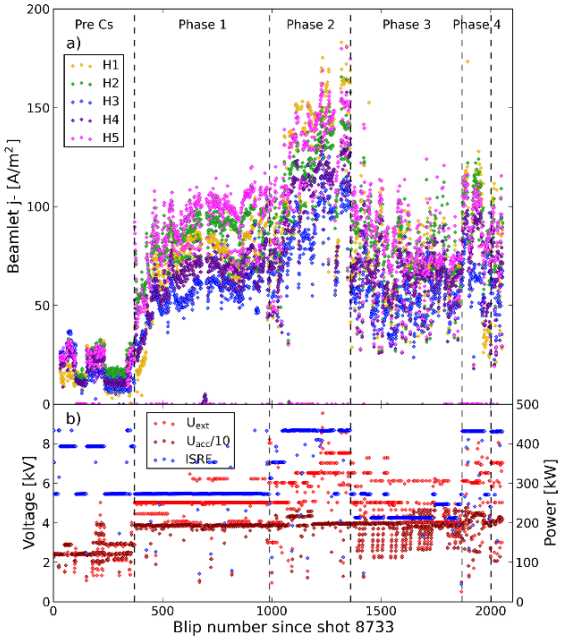

Fig 11. a) BCM DC current during campaign S21, b) SPIDER plant parameters. After pre cesium, phase operations are split into: phase 1 – initial ceasiation at 4x60 kW, phase 2 – operation at 4x100 kW, parameter scans at 4x45 kW, phase 4 – operation at 4x100 kW, phase 5 (not labelled) – deuterium.

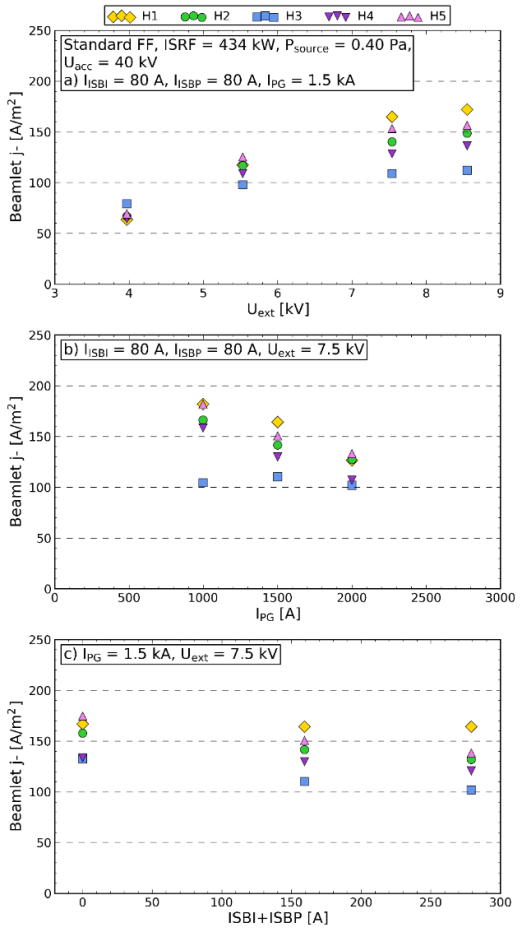

Fig. 12. a) Extraction voltage, b) filter field current and c) bias current scans for the standard FF configuration with cesium.

extraction voltages, the inhomogeneity of the available H- becomes more evident, partially influenced by the magnetic drifts, which increase with the total bias.

Due to limitations on the maximum Acceleration Grid Power Supply (AGPS) voltage at high power the parameter scans were not performed at optimal U_{acc}/U_{ext} (around 10), which has a negative impact on the beam optics. During phase 3 of the cesium campaign scans were performed at lower RF power (45-60 kW) so that U_{ext} and U_{acc} could be set at lower values and still have a saturated beamlet current. Analysis of the BCM data from these scans will be presented in further studies.

REFERENCES

[1] G. Serianni *et al*, "SPIDER in the roadmap of the ITER neutral beams," *Fusion Eng. Des.*, vol. 146, pp. 2539-2546, Sept. 2019, doi: 10.1016/j.fusengdes.2019.04.036.

[2] F. Gasparini, M. Recchia, M. Bigi, T. Patton, A. Zamengo, E. Gaio., "Investigation on stable operational regions for SPIDER RF oscillators," *Fusion Eng. Des.*, vol. 146, pp. 2172–2175, Sept. 2019, doi: 10.1016/j.fusengdes.2019.03.145.

[3] Y. I. Belvenko, G. I. Dimov, V. G. Dudnikov, "A powerful injector of neutrals with a surface-plasma source of negative ions," *Nucl. Fusion*, vol. 14, no. 1, pp. 113-114, Jan. 1974.

[4] G. Serianni *et al*, "First operation in SPIDER and the path to complete MITICA," *Rev. Sci. Instrum.*, vol. 91, Feb. 2020, Art. no. 023510, doi: 10.1063/1.5133076.

[5] M. Pavei *et al*, "SPIDER plasma grid masking for reducing gas conductance and pressure in the vacuum vessel," *Fusion Eng. Des.*, vol. 161, Dec. 2020, Art. no. 112036, doi: 10.1016/j.fusengdes.2020.112036.

[6] A.Pimazzoni *et al*, "Assessment of the SPIDER beam features by diagnostic calorimetry and thermography," *Rev. Sci. Instrum.*, vol. 91, Mar. 2020, Art. no. 033301, doi: 10.1063/1.5128562.

[7] T. Patton *et al*, "Design and development of a diagnostic system for a non-intercepting direct-measure of the SPIDER ion source beamlet current," to be submitted.

[8] https://www.lem.com/en/ctsr-03p.

[9] M. Ugoletti, M. Agostini, M. Brombin, F. Molon, R. Pasqualotto, G. Serianni, "First results of SPIDER beam characterization through the visible tomography," *Fusion Eng. Des.*, vool. 169, May 2021, Art. no. 112667, doi: j.fusengdes.2021.112667.

[10] A. Pimazzoni *et al*, "Co-extracted electrons and beam inhomogeneity in the large negative ion source SPIDER," *Fusion Eng. Des.*, vol. 168, Jul. 2021, Art. no. 112440, doi: 10.1016/j.fusengdes.2021.112440.